ISSN 1674-1056
http://cpb.iphy.ac.cn
http://iopscience.iop.org/cpb
中国物理 B
Chinese Physics
中国物理
Chinese Physics B

Anisotropic photoresponse of layered rhenium disulfide synaptic transistors

Chunhua An(安春华), Zhihao Xu(徐志昊), Jing Zhang(张璟), Enxiu Wu(武恩秀), Xinli Ma(马新莉), Yidi Pang(庞奕荻), Xiao Fu(付晓), Xiaodong Hu(胡晓东), Dong Sun(孙栋), Jinshui Miao(苗金水), and Jing Liu(刘晶)

Citation: Chin. Phys. B, 2021, 30 (**8**): 088503. DOI: 10.1088/1674-1056/abff26
Journal homepage: http://cpb.iphy.ac.cn; http://iopscience.iop.org/cpb

What follows is a list of articles you may be interested in

High performance Cu_2O film/ZnO nanowires self-powered photodetector by electrochemical deposition

Deshuang Guo(郭德双), Wei Li(李微), Dengkui Wang(王登魁), Bingheng Meng(孟兵恒), Dan Fang(房丹), Zhipeng Wei(魏志鹏)

Chin. Phys. B, 2020, 29 (**9**): 098504. DOI: 10.1088/1674-1056/aba610

Theoretical analysis for AlGaN avalanche photodiodes with mesa and field plate structure

Ke-Xiu Dong(董可秀), Dun-Jun Chen(陈敦军), Qing Cai(蔡青), Yan-Li liu(刘燕丽), Yu-Jie Wang(王玉杰)

Chin. Phys. B, 2020, 29 (**8**): 088502. DOI: 10.1088/1674-1056/ab90f1

Total dose test with *γ*-ray for silicon single photon avalanche diodes

Qiaoli Liu(刘巧莉), Haiyan Zhang(张海燕), Lingxiang Hao(郝凌翔), Anqi Hu(胡安琪), Guang Wu(吴光), Xia Guo(郭霞)

Chin. Phys. B, 2020, 29 (**8**): 088501. DOI: 10.1088/1674-1056/ab9286

Photovoltaic effects in reconfigurable heterostructured black phosphorus transistors

Siqi Hu(胡思奇), Ruijuan Tian(田睿娟), Xiaoguang Luo(罗小光), Rui Yin(殷瑞), Yingchun Cheng(程迎春), Jianlin Zhao(赵建林), Xiaomu Wang(王肖沐), Xuetao Gan(甘雪涛)

Chin. Phys. B, 2018, 27 (**12**): 128502. DOI: 10.1088/1674-1056/27/12/128502

Analysis on high speed response of a uni-traveling-carrier double hetero-junction phototransistor

Jiang Zhi-Yun, Xie Hong-Yun, Zhang Liang-Hao, Zhang Wan-Rong, Hu Rui-Xin, Huo Wen-Juan

Chin. Phys. B, 2015, 24 (**4**): 048504. DOI: 10.1088/1674-1056/24/4/048504

SPECIAL TOPIC — Optical field manipulation

Anisotropic photoresponse of layered rhenium disulfide synaptic transistors

Chunhua An(安春华)[1,†], Zhihao Xu(徐志昊)[1,2,†], Jing Zhang(张璟)[1], Enxiu Wu(武恩秀)[1], Xinli Ma(马新莉)[1], Yidi Pang(庞奕荻)[1], Xiao Fu(付晓)[2], Xiaodong Hu(胡晓东)[1], Dong Sun(孙栋)[3], Jinshui Miao(苗金水)[2,‡], and Jing Liu(刘晶)[1,§]

[1] *State Key Laboratory of Precision Measurement Technology and Instruments, School of Precision Instruments and Opto-electronics Engineering, Tianjin University, Tianjin* 300072, *China*

[2] *State Key Laboratory of Infrared Physics, Shanghai Institute of Technical Physics, Chinese Academy of Sciences, Shanghai* 200083, *China*

[3] *International Center for Quantum Materials, School of Physics, Peking University, Beijing* 100871, *China*

(Received 21 March 2021; revised manuscript received 6 May 2021; accepted manuscript online 8 May 2021)

Layered ReS_2 with direct bandgap and strong in-plane anisotropy shows great potential to develop high-performance angle-resolved photodetectors and optoelectronic devices. However, systematic characterizations of the angle-dependent photoresponse of ReS_2 are still very limited. Here, we studied the anisotropic photoresponse of layered ReS_2 phototransistors in depth. Angel-resolved Raman spectrum and field-effect mobility are tested to confirm the inconsistency between its electrical and optical anisotropies, which are along 120° and 90°, respectively. We further measured the angle-resolved photoresponse of a ReS_2 transistor with 6 diagonally paired electrodes. The maximum photoresponsivity exceeds 0.515 $A\cdot W^{-1}$ along *b*-axis, which is around 3.8 times larger than that along the direction perpendicular to *b* axis, which is consistent with the optical anisotropic directions. The incident wavelength- and power-dependent photoresponse measurement along two anisotropic axes further demonstrates that *b* axis has stronger light–ReS_2 interaction, which explains the anisotropic photoresponse. We also observed angle-dependent photoresistive switching behavior of the ReS_2 transistor, which leads to the formation of angle-resolved phototransistor memory. It has simplified structure to create dynamic optoelectronic resistive random access memory controlled spatially through polarized light. This capability has great potential for real-time pattern recognition and photoconfiguration of artificial neural networks (ANN) in a wide spectral range of sensitivity provided by polarized light.

Keywords: ReS_2, in-plane anisotropy, anisotropic photoresponse, phototransistor

PACS: 85.60.Dw, 84.32.Ff, 85.25.Hv **DOI:** 10.1088/1674-1056/abff26

1. Introduction

Planar single/multi-layer structure of layered materials, such as graphene and transition metal dichalcogenides (TMDs), is of great promise for optoelectronic and spintronic applications.[1–3] In this category of two-dimensional (2D) systems, ReS_2 has recently gained attention for its unique optical and electrical properties. Due to the lack of interlayer registry and weak interlayer coupling, ReS_2 behaves electronically and vibrationally decoupled, leading to a retention of direct bandgap of 1.5 eV from bulk to monolayer.[4,5] According to the previous works, few-layer ReS_2-based transistors show n-type behavior with electron mobility of around 40 $cm^2\cdot V^{-1}\cdot s^{-1}$, while the photodetectors exhibit gate-tunable photoresponsivity up to 16.14 $A\cdot W^{-1}$ and external quantum efficiency reaching 3168%.[6,7] Besides, the unique 1-T structure of ReS_2 results in high anisotropic carrier mobility and matter–light interaction along different crystal axes.[4] However, the controversial inconsistency between the priciple axes of electrical and optical anisotropies causes many confusion in developing angle-resolved opto-electronic devices, such as polarization sensitive photodetectors, photo-modulated neuromorphic devices.[7,8] Therefore, a systematic study on the anisotropic photoresponse of ReS_2 is highly demanded.

In this report, we aim to understand the photoresponse anisotropy of ReS_2, as well as its relationship with the electrical and optical anisotropies, to provide helpful information to design polarization-sensitive optoelectronic devices. Firstly, polarizd Raman spectroscopy is used to identify the two optical priciple axes of exfoliated ReS_2 flake, which is along *b* axis and the direction perpendicular to the *b* axis, respectively. Then, a field-effect transistor (FET) is fabricated based on the same ReS_2 flake with 12 electrodes (6 pairs of diagonal electrodes), to identify its two electrical priciple axes, which is along *b* and *a* axes, respectively, demonstrating the inconsistency of optical and electrical anisotropy. We further test the photoresponses of the ReS_2-based 12-electrode transistor along different directions under light illumination with

†These authors contributed equally to this work.

‡Corresponding author. E-mail: jsmiao@mail.sitp.ac.cn

§Corresponding author. E-mail: jingliu_1112@tju.edu.cn

© 2021 Chinese Physical Society and IOP Publishing Ltd

different wavelengths and incident power. The results indicate that the photoresponse anisotropy agree with the optical anisotropy, which may be attributed to the fact that the light–matter interaction plays a major role in the photoresponse. Finally, we demonstrate a angle-resolved neromorphic device stimulated by polarized light, the preliminary results of which suggests the ReS_2 a promising material for multi-bit in-memory computing devices. Compared with most of the neuromorphic devices with synaptic functions using electric signals to stimulate, photonic signals possess many advantages, such as high bandwidth and ultrafast propagation speed.[9–12] Combining photonic stimuli with electric ones in synaptic devices has numerous advantages; it leads to the development of novel optoelectronic devices with mixed-electro-optical operations, such as synthetic retinas and optoelectronic interfaces for integrated photonic circuits.[13,14]

2. Results and discussion

Figure 1(a) shows the schematic diagram of a ReS_2 FET, which was fabricated by mechanically exfoliating a few-layered ReS_2 flake from its bulk counterpart and transferring onto a Si/SiO_2 substrate (the thickness of the SiO_2 is 90 nm). E-beam lithography, metal evaporation, and lift-off processes are sequentially perfomed to deposit 12 electrodes comprising 5-nm Cr/45-nm Au on the ReS_2 flake. The 12 electrodes are spaced 30° apart from each other, which enable the collection of photo-generated carriers along 6 pairs of diagonally paired electrodes. Figure 1(b) presents the optical image of the fabricated ReS_2 transistor device, in which the *b* axis of the ReS_2 flake is labled as the direction of 90°. We distinguishe the crystallographic orientation of ReS_2 by angle resolved polarized Raman spectroscopy, which is a nondestructive techniques widely used in a variety of applications including studying strain-induced changes in the electronic structure of graphene and determining the orientation of BP.[15,16] Figure 1(c) shows the Raman spectra of the ReS_2 flake excited by a linearly polarized light, as it is polarized along different directions. Along all directions, the Raman spectra exhibit feature modes of ReS_2, which are consistent with previous reports. However, by shifting the polarization angle of the incident light, the intensity of the Raman modes changes significantly such as mode V, which represents the out-of-plane vibrations of the sulfur atoms along with in-plane vibrations of the rhenium atoms in the direction of the *b* axis.[16] Figure 1(d) plots the intensity of mode V in the polar coordinate. It exhibits a maximum intensity at the angle of $\sim 90°$, which is parallel to the *b* axis of the ReS_2 flake as shown in Fig. 1(b), while it has the minimum intensity at an angle of 180°, which is perpendicular to the *b* axis. This result indicates the prominent optical anisotropy of the ReS_2 flake with an anisotropic angle of 90°.

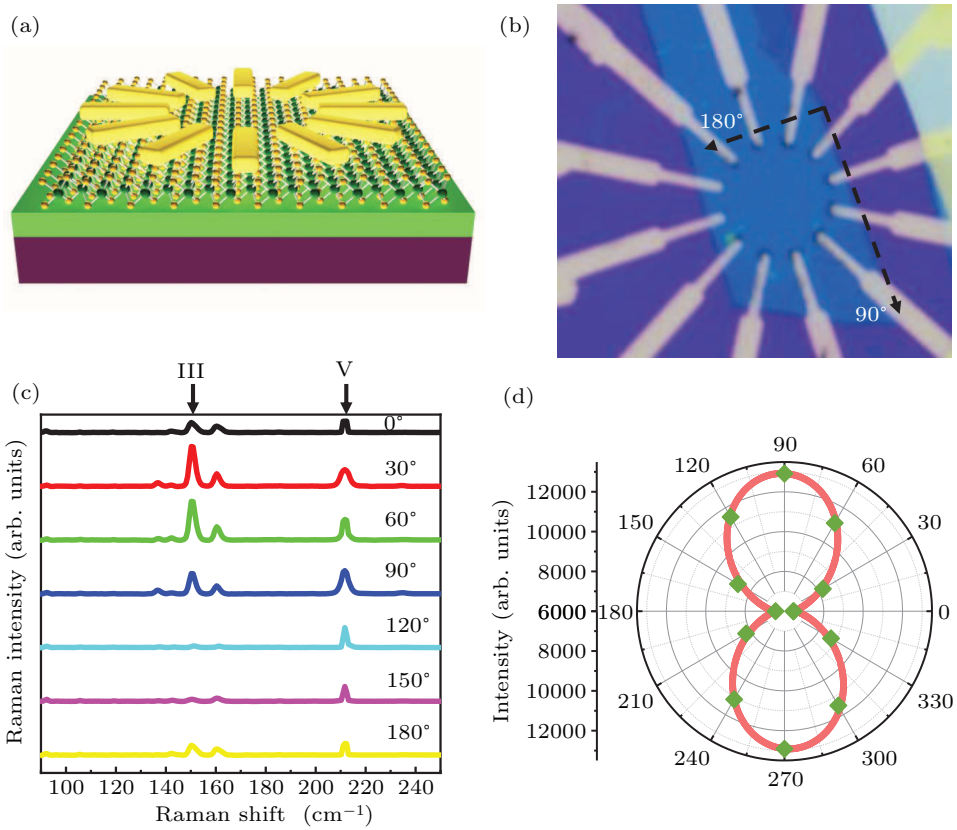


Fig. 1. Raman spectra for ReS_2 transistors with 12 electrodes: (a) schematic diagram of ReS_2 transistor with 12 electrodes, (b) optical image of the ReS_2 transistor with 12 electrodes spaced 30° apart, (c) detailed Raman spectra of the ReS_2 sample with different rotation angles under 514.5-nm laser excitation, (d) polar plots of angle-resolved polarized Raman scattering intensities of mode V under 514.5 nm.

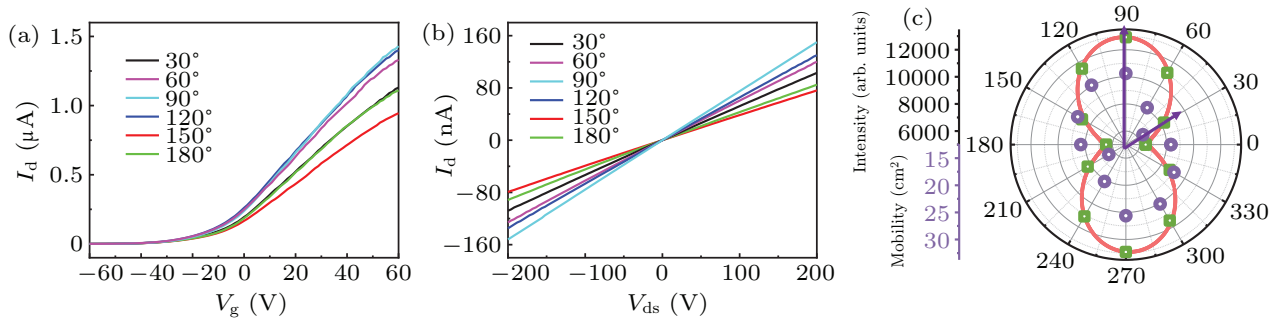


Fig. 2. Angle-resolved DC conductivity of the ReS_2 transistor. (a) Room temperature transfer curves of the ReS_2 transistor measured by the diagonally paired electrodes along different directions. (b) Output characteristics of the device measured by the diagonally paired electrodes along different directions. (c) Angle-resolved polarized Raman scattering intensities and field-effect mobilities (purple dots) of the same ReS_2 device plotted in polar coordinates.

To quantify the orientation-dependent mobility, the electrical transport measurement of the ReS_2 FET was carried out at room temperature. Figure 2(a) presents the transfer curves of the device along 6 orientations defined by each diagonally paired electrodes. Along all the 6 directions, strong negative gate bias depletes the n-type ReS_2 flake and decreases the channel current, while strong positive gate voltage shifts the ReS_2 channels into the accumulation region and increases the channel current, resulting in a current on-off ratio exceeding 10^4. However, the on-state current varies with directions, with the maximum and minimum values achieved at 90° and 150°, respectively. The output characteristic curves are plotted in Fig. 2(b), in which the channel current changes linearly with the source–drain bias, indicating Ohmic contact at the ReS_2 and Cr/Au interfaces. Additionally, the value of the channel current also changes with the crystal orientations, which is completely consistent with the trend of the transfer curves. We further extract the field-effect mobilities along each direction, which achieves the maximum and minimum values of 25.62 $cm^2 \cdot V^{-1} \cdot s^{-1}$ and 16.13 $cm^2 \cdot V^{-1} \cdot s^{-1}$ at 90° (*b* axis) and 150° (*a* axis) respectively, by

$$\mu = \frac{L}{WC_{ox}V_{ds}} \frac{dI_{ds}}{dV_g}, \tag{1}$$

where $L = 13$ μm is the channel length, $W = 1.5$ μm is the channel width, and C_{ox} is the capacitance between the channel and the back gate per unit area, which is calculated by

$$C_{ox} = \frac{\varepsilon_0 \varepsilon_r}{d}, \tag{2}$$

where ε_0 is the vacuum permittivity, ε_r is the relative permittivity, and $d = 90$ nm is the thickness of SiO_2 layer, respectively. Figure 2(c) plots the field-effect mobility of the ReS_2 device in a polar coordinate. Combining the results of polarized Raman spectra and electrical measurement, it can be concluded that the *b* axis of ReS_2 crystal has the maximum intensity of Raman shift and the highest field-effect mobility. The direction of the minimum intensity of Raman separates 30° away from the direction with the lowest field effect mobility (*a* axis). These results are consistent with previous work reported by Liu *et al.*,[17–19] and consistent with the views of crystal fracture shown in Fig. 1(b).

Figure 3(a) presents the photocurrent (I_p) of the ReS_2 transistor as a function of gate bias along different crystal orientations, by substracting the channel current value under dark condition (I_{dark}) from the value under light illumination ($I_{illumination}$). The original transfer characteristics of the ReS_2 device under both the dark and illuminated states along *b* axis are shown in the Supporting information. The incident light is 550 nm with incident power of 1.096 mW. When V_g is swept from −60 V to 60 V ($V_{ds} = 200$ mV), the photocurrent of the device increases to a maximum value and then decreases. By comparing the peak photocurrent along different directions, the highest photocurrent is reached at 90° (*b* axis), while the minimum photocurrent is appeared at 180°, which is consistent with the optical anisotropic direction. Such variation of photocurrent with gate bias can be illustrated by the band alignment modulation in Figs. 3(e)–3(g). Firstly, when gate voltage is −60 V, the Fermi level E_F of ReS_2 shifts to the middle of its bandgap, resulting in increased Schottky barrier height between the electrodes and the ReS_2 flake to suppress the transport of the generated photo carriers, and thus, the photocurrent (see Fig. 3(e)). As the gate voltage increases, E_F moves to the conduction band of the ReS_2, and thus, the Schottky barrier height decreases as shown in Fig. 3(f), which leads to easier carrier transport from ReS_2 to electrode and increase photocurrent until it reaches the maximum value. By continuously increasing the gate bias, E_F approaches the conduction band, and the dark current is so high that limits the number of photo-generated carriers and thus photocurrent. The high concentration of carriers also decreases the transport speed of the photon generated carriers due to the increased scattering, which further decreases the photocurrent. The generated photocurrent can be attributed to two mechanisms: 1) the source–drain bias separates the photon-generated electron–hole pairs, and forms the photocurrent; 2) the photon excited carriers are partially traped by the defect states at both the ReS_2 and the interface between ReS_2 and Si/SiO_2 substrate, generating the photogating effect to modulate the photocurrent of the chan-

nel. In Fig. 3(a), the gate voltage corresponding to the maximum carrier mobility is larger than the gate voltage corresponding to the peak photocurrent in the case of the carrier without lightunder illumination. It demonstrates that photogating is the dominant effect. Figure 3(b) presents the photocurrent along different directions as a function of source–drain voltages with gate voltage of −40 V to maintain relatively high photocurrent as compared to the dark current. As expected, the photocurrent differs along different directions, which achieves a maximum difference factor of 3.8 along 90° and 180° . This trend is also consistent with the ReS_2 optical anisotropic angle. We then calculate the photoresponsivity R_p of the ReS_2 transistor, which is defined as

$$R_p = I_p/P_{light},$$

where R_p is the photoresponsivity and P_{light} is the power of the illumination laser. Figure 3(c) shows the photoresponse under drain voltages of 200 mV as a function of different diagonally electrode angles. The data can be fitted by a sinusoidal function and the highest photoresponsivity is around 0.515 A/W along *b* axis.

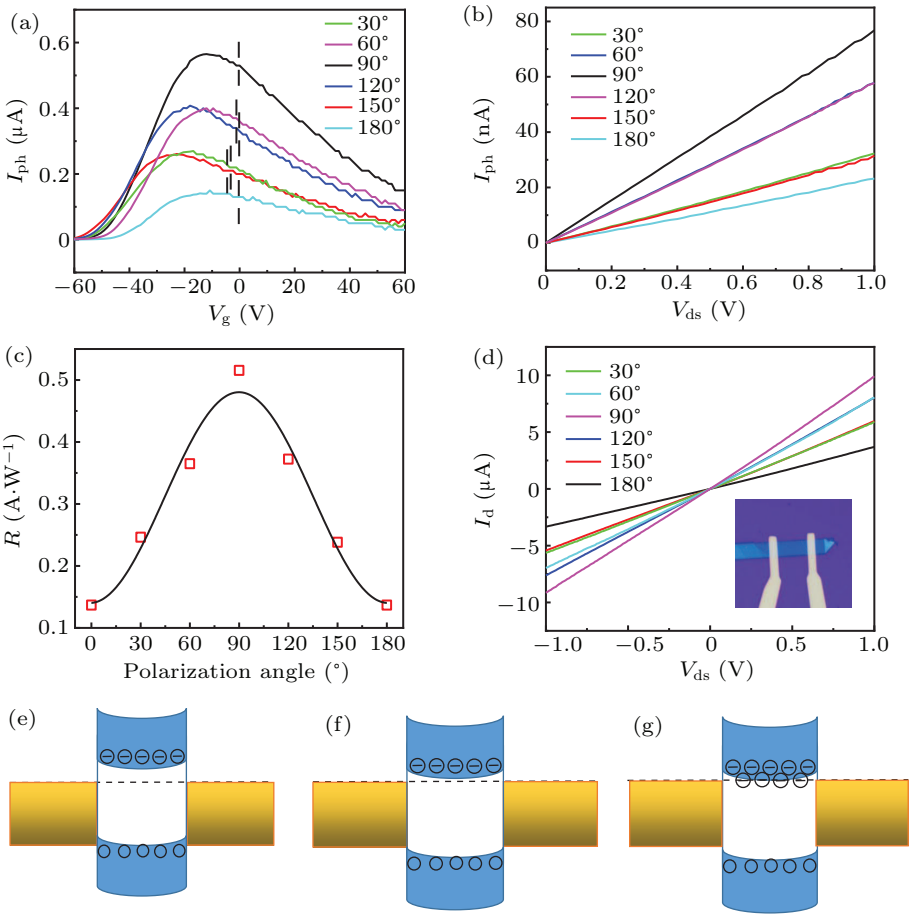


Fig. 3. Photocurrent generation mechanism in ReS_2 field-effect transistors. (a) Room temperature angle-resolved photocurrent measured as a function of back-gate voltage under illumination. (b) Room temperature angle-resolved photocurrent measured as a function of V_{ds} at −40-V back gate voltage. (c) Photoresponsivity as a function of the angle defined by diagonally paired electrodes. (d) The photocurrent change as a function of V_{ds} under different polarization light illuminations. Inset: Optical image of the transistor used in polarized illumination test. (e), (f), (g) Schematics of device band profiles for $V_g < V_{th}$, $V_g \approx V_{th}$, and $V_g > V_{th}$, respectively. E_F, Fermi level.

To verify the anisotropic photosensitivity, we fabricate a two-electrode ReS_2 device with the diagonally paired electrodes along *b* axis. Figure 3(d) plots the source–drain current of this device as a function of source–drain bias under illumination of light polarized along different angles. The optical image of the device is shown in the inset of Fig. 3(d). The polarization of the light is controlled via the combination of one half wave plate and a polarizer. By rotating the polarizer and keeping the incident power constant, the photocurrent of the device changes dramatically. The variation trend of the photocurrent with the incident light polarization angle is consistent with the trend tested by 12-electrode device, which reaches the maximum and minimum photocurrents along the 90° (*b* axis) and 180°, respectively.[20–22]

We further probe the photoelectric nature of the ReS_2 FET by performing I_{ds}–V_{gs} measurements at room temperature under light illumination of different wavelengths and power, as presented in Fig. 4. In Figs. 4(a) and 4(b), a standard wavelength-tunable laser is iluminated at a 4-electrode ReS_2 device (two diagonally paired electrodes are along 90° and

180°, respectively) with incident power kept at 1.096 mW. The V_{ds} is 200 mV and gate voltage is swept from −60 V to 10 V. In this gate bias regime, the photocurrent keeps increasing, and gradually becomes saturated. Channel current increases differently when incident light ranged from 450 nm to 750 nm. The wavelength-dependent transfer curve groups are also different along 90° and 180°. In addition, both channel currents reach the maximum value when the incident wavelength is 550 nm, which matches the bandgap of ReS_2. However, the effect of the wavelength of incident light is more prominent on the channel current along 90° than along 180°. Figures 4(c) and 4(d) show the I_{ds}–V_{gs} plots of the device measured along 90° and 180°, respectively, with different powers of illumination. As expected, the channel current increases with the incident power along both 90° and 180°, showing a strong dependence on the laser power. Again, the current along 90° has a larger change with incident power than the current along 180°, due to the stronger light-cyrstal interaction along 90° than 180°.

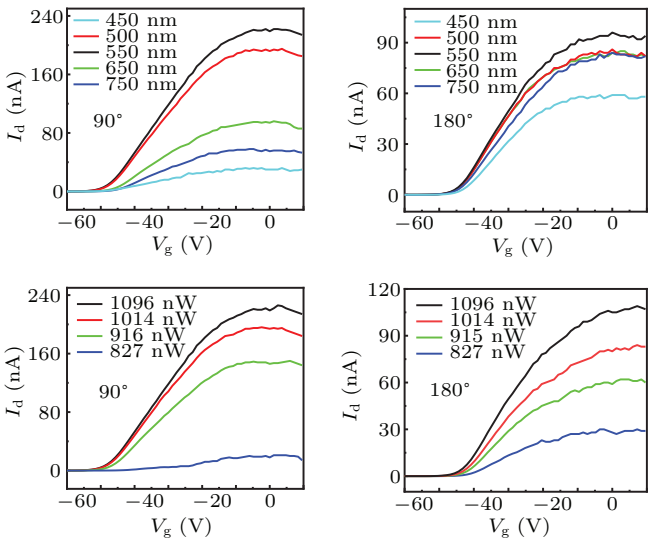


Fig. 4. Wavelength- and power-dependent photoelectric properties of ReS_2 transistor. (a), (b) The I_{ds}–V_g curves of the device, when the ilumination light is polarized along 90° (a) and 180° (b), respectively, with incident wavelength varying from 450 nm to 750 nm. The incident power is set at 1.096 mW. (c), (d) The I_{ds}–V_g curves of the device, when the ilumination light is polarized along 90° (c) and 180° (d), respectively, with incident power varying from 827 nW to 1096 nW. The incident wavelength is fixed at 550 nm.

The above anisotropic optoelectronic behaviors of the ReS_2 device indicate that it a promising anistropic optoelectronic memory, which can be programmed by polarized optical stimuli and read out by orientation-dependent electrical measurements.[23–26] ReS_2 phototransistor with two diagonally paired electrodes along 90° and 180° is fabricatated as shown in Fig. 5(a). The electrodes paralleled to the *b* axis is assigned as parallel direction, while the other pair of electrodes is assigned as perpendicular direction. Figure 5(b) shows the AFM image of the ReS_2 flake with thickness around 8 nm. The presence of surface contamination as shown in the AFM image may come from the contamination during fabrication process and ambient environment, which may provide trap states to trap photon excited carriers.[27–29] Figures 5(c) and 5(d) show the dynamic photoresponse of this ReS_2 FET to weak fluorescent lamp with the source–drain bias voltage of 2.0 V and gate bias V_{bg} at −50 V (to reduce the dark current). By turning on and off the fluorescent lamp at one-second intervals, source–drain currents along both directions increase under illumination and decrease without illumination. However, the final channel current level becomes higher than the level before light illumination. Therefore, after applying around 25 identical light illumination pulses successively, the channel current increases steadily to a level that can be easily distinct from the original level, and exhibits non-volatile behavior. As expected, after 25 light pulses stimuli, the current along 90° is much higher than that along 180° due to the stronger light–ReS_2 interaction along 90° than 180°. In this way, the ReS_2 phototransistor can be used as multi-bit flash memory and synaptic transistor. In a synaptic transistor, the drain terminal can be used to imitate the postsynaptic neuron. The synaptic weight can be represented by I_{ds}, which is named postsynaptic current (PSC) in the synaptic transistor context. From results in Figs. 5(c) and 5(d), the PSC gradually increased with the increase of the number of pulses, which suggests that the channel conductance can be gradually modulated to higher states. As mentioned in Fig. 3(b), when the spikes were removed, the PSC values returned to lower states, but not completely disappeared. As a result, the synaptic weights can be further enhanced by increasing the number of pulses. In this way, the photonic stimuli can be used to set the state of the device, and the electric stimuli can be used in the reset process which is shown in Fig. 5(e). It should be noted that the minimal width and interval of the photonic pulses is 1 s due to the limitation of our light source. At first, the current is relatively low, then on application of a series of consecutive light pulses, the current of the ReS_2 transistor increases gradually due to the photogating effect, which can be used to mimic the potentiation of the synaptic strength. In this process, the gate voltage kept on −50 V to reduce the dark current. Afterward, under the positive electric pulse of 50 V, the photocarriers which are located in the trap state are released. When the electric stimuli disappears, the current in the ReS_2 gradually is decreased to the initial state voltage corresponding to the habituation behavior. It also should be noticed that we finished the reset process by applying the same electric stimuli with different time interval (2 s, 3 s, 4 s) due to the lack of the electric pluses generator. Finally, the memory function with optical write–electric erase can be realized in the ReS_2 transistors. Those properties of our s photogating effect 3-terminal device could provide the potential to simulate signal communication between a sensory afferent neuron and a neuron in the central nervous system. Besides, the additional gate voltage provided by trapped

photo-generated carriers enablesour ReS_2 FET to be a potential memory device. Furthermore, the different conductances of different directions reflect the FETs can be promising candidates for the multi-bits memory device.

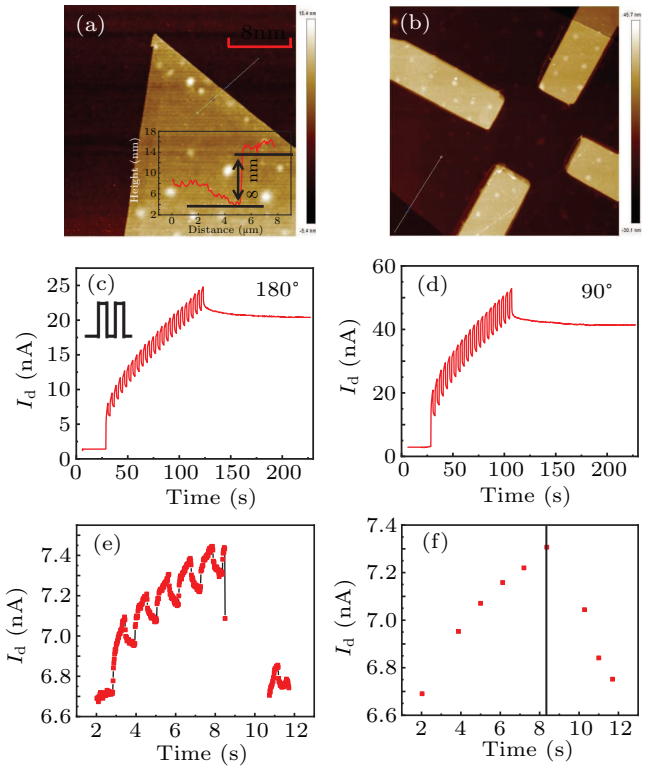


Fig. 5. Time-dependent I_{ds} of the ReS_2 transistor with laser illumination polarized along different directions. (a) and (b) AFM images of the ReS_2 flake. (b) Enlarged AFM image of the ReS_2 flake in panel (a). Inset is the height profile of the ReS_2. The height was 8 nm. (c), (d) The real-time response characteristics of the ReS_2 FET in panel (a) with the bias voltage of 2.0 V. V_{bg} is fixed at −50 V. The polarized angles of the incident light is at 180° (c) and 90° (d), respectively. (e) Photonic potentiation and electric habituation in the ReS_2 synaptic transistors. Set: photonic pulse (fluorescent lamp and width: 1 s). Reset: electric pulse (50 V). Reading voltage: −50 V.

3. Conclusions

With the combination of polarization Raman spectroscopy and angle-resolved electrical measurements, we successfully revealed the in-plane optical and electrical anisotropies of 2D layered ReS_2. The ratio of anisotropic photo-electronics can reach as high as 3.8, which holds great promise for the development of angle-resolved optoelectronic and electronic devices. The systematic photoresponse experiments performed on ReS_2-based 12-electrode FET demonstrated the anisotropic axes of photoresponse agree with the optical anisotropic axes due to the key role of light–matter interaction played in the generation of photocurrent. Furthermore, an angle-resolved synaptic transistor is developed based on the ReS_2 device stimulated by polarized light, which shows potential applications in simulating nervous systems and artificial intelligent chips.

References

[1] Freitag M 2008 *Nat. Nanotechnol.* **3** 455
[2] Geim A K and Grigorieva I V 2013 *Nature* **499** 419
[3] Liu Y, Weiss N O, Duan X, Cheng H C, Huang Y and Duan X F 2016 *Nat. Rev. Mater.* **1** 16042
[4] Tongay S, Sahin H, Ko C, Luce A, Fan W, Liu K, Zhou J, Huang Y S, Ho C H, Yan J, Ogletree D, Aloni S, Ji J, Li S, Li J, Peeters F M and Wu J 2104 *Nat. Commun.* **5** 3252
[5] Horzum S, Ćakır, D, Suh J, Tongay S, Huang Y S, Ho C H, Wu J, Sahin H and Peeters F M 2014 *Phys. Rev. B* **89** 155433
[6] Zhang E, Jin Y, Yuan X, Wang W, Zhang C, Tang L, Liu S, Zhou P, Hu W and Xiu F 2015 *Adv. Functl. Mater.* **25** 4076
[7] Liu E, Long M, Zeng J, *et al*. 2016 *Adv. Funct. Mater.* **26** 1938
[8] Liu F, Zheng S, He X, *et al*. 2016 *Adv. Funct. Mater.* **26** 1169
[9] Ríos C, Stegmaier M, Hosseini P, Wang D, Scherer T, Wright C D, Bhaskaran H and Pernice H 2015 *Nat. Photon.* **9** 725
[10] Liu Y, Guo J, Song W, Wang P, Gambin V, Huang Y and Duan X 2021 *Small Struct.* **2** 2000039
[11] Zhong H, Sun Q, Li G, Du J, Huang H, Guo E, He M, Wang C, Yang G, Ge C and Jin K 2020 *Chin. Phys. B* **29** 040703
[12] Wang X, Ge C, Li G, Guo E, He M, Wang C, Yang G and Jin K 2020 *Chin. Phys. B* **29** 098101
[13] Ho, C H and Huang C E 2004 *J. Alloys Compd.* **383** 74
[14] Dumcenco D O and Huang Y S 2007 *J. Appl. Phys.* **102** 083523
[15] Fang C M, Wiegers G, Haas C and Groot R A de 1997 *J. Phys.: Condens. Matter* **9** 4411
[16] Thakar K, Mukherjee B, Grover S, Kaushik N, Deshmukh M and Lodha S 2018 *ACS Appl. Mater. Interfaces* **10** 36512
[17] Guo Q, Pospischil A, Bhuiyan M, *et al*. 2016 *Nano Lett.* **16** 4648
[18] Huang M, Yan H, Heinz T and Hone J 2010 *Nano Lett.* **10** 4074
[19] Xia F, Wang H and Jia Y 2014 *Nat. Commun.* **5** 4458
[20] Chenet D A, Aslan O B, Huang P, Fan C, Zande A, Heinz T and Hone J 2015 *Nano Lett.* **15** 5667
[21] Ovchinnikov D, Gargiulo F, Allain A, Pasquier D, Dumcenco D, Ho C H, Yazyev O and Kis Andras 2016 *Nat. Commun.* **7** 12391
[22] Liu E, Fu Y, Wang Y, *et al*. 2015 *Nat. Commun.* **6** 6991
[23] Xu M, Gu Y, Peng R, Young N and Li Mo 2017 *Appl. Phys. B* **123** 130
[24] He H, Yang R, Zhou W, Huang H, Xiong J, Gan L, Zhai T and Guo X 2018 *Small* **14** 1800079
[25] Jin H, Xin S, Chuang C, Li W, Wang H, Zhu J, Xie H, Zhang T, Wan Y, Qi Z, Yan W, Lu Y, Chan T, Wu X, Goodenough J, Ji H and Duan X F 2020 *Science* **370** 192
[26] Zhao Y, Liu B, Yang J, He J, and Jiang J 2020 *Chin. Phys. Lett.* **37** 088501
[27] Guo C, Wang B, Xia W, Guo Y and Xue J 2019 *Chin. Phys. Lett.* **36** 078501
[28] Ho C H 2013 *Cryst. Struct. Theory Appl.* **02** 65
[29] Ho C H, Yen P C and Huang Y S 2002 *Phys. Rev. B* **66** 245207